Journal of Microelectronics and Electronic Packaging (2012) **9**, 187-198

ISSN: 1551-4897

Inkjet Printing Technology: A Novel Bottom-up Approach for Multilayer Ceramic Components and High Definition Printed Electronic Devices

C. Dossou-Yovo,[1,*] M. Mougenot,[1] E. Beaudrouet,[1] M. Bessaudou,[1] N. Bernardin,[1] F. Charifi,[1] C. Coquet,[1] M. Borella,[1] R. Noguera,[1] C. Modes,[2] M. Lejeune,[3] P. Laurier,[4] D. Detemmerman,[4] P. Escure,[5] H. Laville,[5] N. Delhotes,[6] and S. Verdeymes[6]

Abstract—**This paper describes the methodology of thick film and multilayer ceramic capacitor (MLCC) component manufacturing by inkjet printing. The printing unit is a CeraDrop 3D multimaterial inkjet printer. Aqueous conductive and dielectric inks were formulated according to the printhead specifications in terms of viscosity, surface tension, particle size, and sedimentation. Jetting behavior was controlled and optimized to reach the best droplet characteristics with regard to the design. The numerical processing simulation tool helps to control the printing job and to identify potential beneficial issues during the processing. Therefore, printing parameters (droplet spreading, layer thickness, filling strategy, layer drying, etc.) were optimized according to material and component design characteristics. In this way, high definition and thin conductive tracks were achieved on an alumina substrate with good electrical properties. Moreover, two printheads were used to successively build 3D multimaterial MLCC components with thin dielectric and conductive layers (i) with good precision of margins compared with traditional processes, and (ii) with very high complex configurations thanks to the flexibility of the inkjet printing process. For both applications, large area components were accessible in a single batch.**

Keywords—**Inkjet printing, MLCC, printed electronics, thick film**

Introduction

Inkjet printing (IJP) is an attractive technology that has become increasingly accepted for a variety of industrial applications for patterning functional materials [1-11]. The prototyping techniques developed up to now for ceramic parts such as stereolithography [12-16], fused deposition modeling [17, 18], and selective laser sintering [19] are characterized by a definition around 150 μm, and do not allow the deposition of different materials on the same layer. Although screen printing, photolithography, and electrochemical deposition have been widely adopted in the microfabrication of conductive features, these processes are time-consuming, complicated, and expensive [20, 21]. Therefore, the inkjet process opens the way to the development of digital multifunctional 2D and 3D fine scale components (Fig. 1). The technology is cost-efficient, can deliver precise quantities of materials [22-28], and allows excellent resolution for material deposition without any contact with the substrate. Thus, the process consists of the deposition of material microdroplets (a few pL) ejected via nozzles to build the successive layers of the 3D structures. This additive approach helps to minimize waste, material consumption, contamination, and processing steps. By adjustment of the aperture of the printhead and the control of the spreading phenomenon of the droplet, we have previously succeeded in achieving fine scale PZT micropillar arrays [30] with a definition around 40 μm, which could potentially be reduced to 10 μm, taking into account the tremendous evolution of the printing field. Moreover, this technique exhibits the additional capability of depositing different materials on the same layer via a multinozzle system. Further, thanks to its high flexibility in terms of design, and because of its capability of depositing different materials with high definition, this technique may be applied in particular to the production of sophisticated microelectronic devices, integrating a metallic connection network (packaging, microactuators, or sensors, etc.). The purpose of this study is to describe the printing job of conductive tracks for thick film application and the manufacture of multimaterial components for MLCC application through drop-on-demand 3D IJP technology. Aqueous nanosilver and dielectric inks were successfully formulated and are suitable for long storage time and for small batch printing. The nanosilver ink is compatible with substrates that allow high-temperature firing. Complex shapes of functional silver and ceramic components were patterned on variable substrates using accurate IJP equipment, namely, the CeraPrinter X-Serie (CeraDrop, Limoges, France).

Received July 30, 2012; Revised November 26, 2012; Accepted December 10, 2012
[1]CeraDrop, Ester Technopole, 32 Rue Soyouz, 87068 Limoges, France
[2]Heraeus, Hanau, Germany
[3]SPCTS, CNRS-UMR 7315, Limoges, France
[4]CMAC, Ronse, Belgium
[5]EuroFarad, Chanteloup-En-Brie, France
[6]XLIM, CNRS, Limoges, France
*Corresponding author; email: c_dossou-yovo@ceradrop.fr

Dedicated Printer

The printing system is a drop-on-demand 3D multimaterial printer dedicated to digital manufacturing of printed electronic components with high accuracy (Fig. 2). The equipment is based on patented technology that can print up to four materials with

doi:10.4071/imaps.338

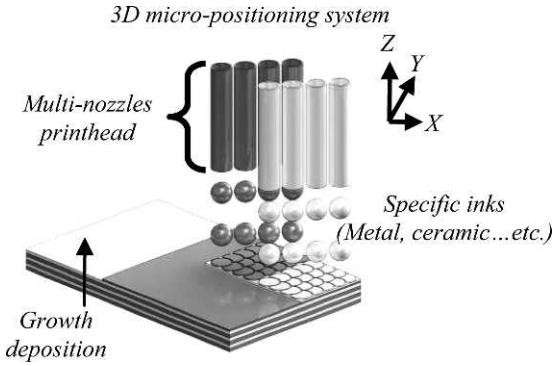

Fig. 1. 3D multimaterial inkjet printing principle.

Fig. 2. CeraPrinter X-Serie.

an embedded curing or drying system. It allows substrate printing up to a size of 305 × 305 mm^2. Droplet analysis (diameter, velocity, jet straightness, clogged nozzles, etc.) is carried out by stroboscopically capturing backlit images of the ejection with a CCD camera. The printing job definition takes into account all the process parameters from CAD files to printing script generation via dedicated CAM software, called CeraSlice. Using a novel bottom-up approach to inkjet technology, the printing parameters can be defined according to material and component design characteristics (splat diameter, layer thickness, filling strategy, droplet pattern, layer drying, etc.) directly on CAD files, with the designer's native software (DXF, Step, Gerber, GDS II, etc.).

Inkjet Printing of Thick Film Components

A. Nanosilver Ink Preparation

With respect to environmental rules, the inks described in this paper are stable and water based inks . The low evaporation rate of water helps to avoid premature nozzle clogging. The different inks were formulated by adding some organic additives such as binders, plasticizers, and surfactants. The selected additives, all miscible with water, help to adjust the physical and chemical properties of the ink (viscosity, surface tension, pH, conductivity, particle size, and stability) to be compatible with the printhead and the IJP process (Table I). Liquid additives were combined directly, whereas solid ones were dissolved in water before mixing with the suspension. The rheological behavior was measured using a Pelletier cone and plate rheometer (TA Instruments AR1500EX). The surface tension was controlled by the Whilhelmy plate method using a Data Physics DCAT21 tensiometer. Conductivity and pH were

Table I
Print Heads and Inkjet Printing Specifications

Particle size (μm)	D90 < 1
pH range	2-12
Conductivity (mS/cm)	<10
Viscosity (mPa·s)	5-20
Surface tension (mN/m)	24-36
Ejection ratio [30]	
Sedimentation rate/8 h (wt.%)	<10

controlled using a Consort C862 instrument. The particle size and distribution were measured by a dynamic light scattering instrument (Brookhaven BIC 90Plus). The particle morphology was analyzed by scanning electron microscopy (MiniMeb Hitachi 3000). The ink stability was measured by evaluating its sedimentation rate as a function of time using the Data Physics DCAT21 tensiometer, which measures the sedimented weight into an emerged cone in the ink.

I. Nanosilver Suspension

The conductive silver ink used in this study is dedicated for printed electronics applications. It was formulated from nanosilver water-based dispersion provided by Heraeus. The physicochemical characteristics of this suspension are summarized in Table II.

The nanosilver dispersion exhibits a high solid content (6.4 vol.% ∼42 wt.%) in water, with an average particle size of 10 nm shown by transmission electron microscopy (Fig. 3) and a monomodal size distribution (Fig. 4).

Consequently, this particle size is perfectly convenient for IJP application and for the selected printhead, for which the nozzle aperture is around 40 μm.

Table II
Nanosilver Suspension Characteristics

Silver content (vol.%-wt.%)	6.4-42
pH	7.8
Conductivity at 25°C (mS/cm)	3.9
Viscosity at 20°C and 1000 s^{-1} (mPa·s)	11.6
Surface tension (mN/m)	59.6
Density	1.6
Sedimentation rate/8 h (wt.%)	4.59

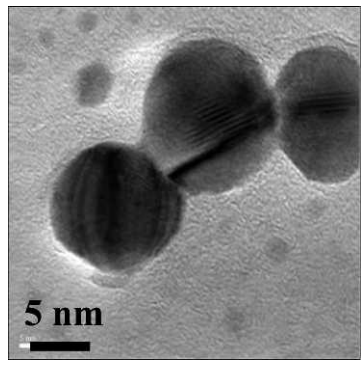

Fig. 3. TEM of nanosilver particle.

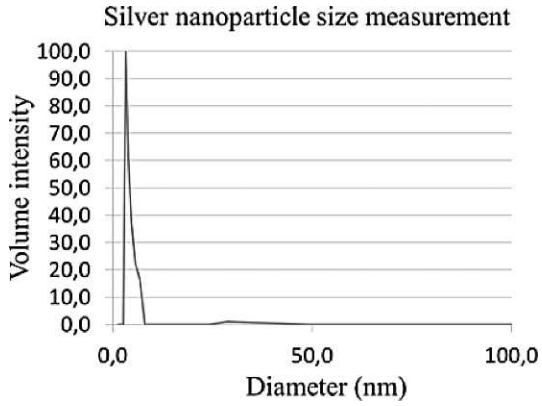

Fig. 4. Nanosilver particle size distribution.

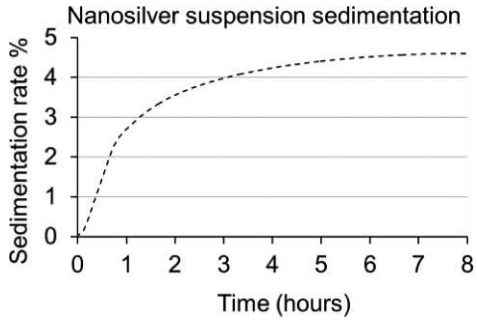

Fig. 5. Nanosilver suspension sedimentation.

Conductivity, pH, and viscosity, at 3.9 mS/cm, 7.8, and 11.6 mPa·s, respectively, are adequate for the IJP specifications (Table I). However, the surface tension appears to be out of the specification optimum. In addition, the suspension appears to be stable, as the sedimentation rate is measured to be 4.9 wt.% within 8 h (Fig. 5).

There is no significant variation of the suspension characteristics over 6 mo. Nevertheless, some batches exhibit rapid coagulation and investigations are underway to understand this aging phenomenon. The material is adapted for both MLCC, in order to be cofired with low-temperature dielectric ceramics, and for thick film applications, where printing occurs on substrates like glass or ceramic substrates and requires high temperature firing (850°C) for the densification of the other thick film material (resistive or insulating layers).

II. Nanosilver Ink Formulation

According to both printhead and IJP requirements, the nanosilver suspension is not adapted to the process especially with regard to the surface tension. Not only the surface tension but also the viscosity must be adjusted by adding some organic additives. The expected colloidal silver ink formulation corresponds to 5 vol.% of Ag, 85 vol.% of water, and 5 vol.% of organic additives (binder, plasticizer, and surfactant), all miscible with water. Even though the suspension viscosity is within the required specification, adding the binder further creates the basis for a consistent droplet with regard to the ejection ratio (2.6) and yields sufficient mechanical strength for the green deposit. Plasticizer helps to avoid cracks in the printed layers. In addition, the presence of surfactant helps the ink's wettability with the nozzle plate and also helps to control the resolution after the droplet impacts on the substrate.

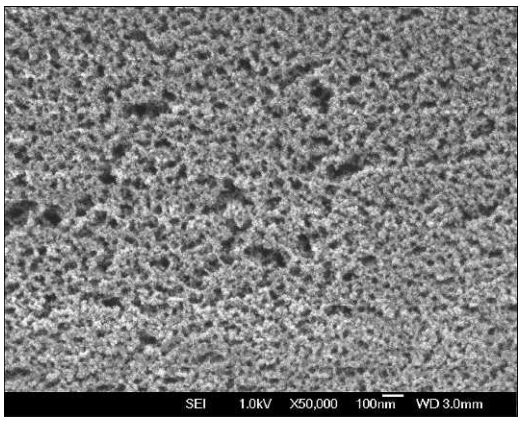

Fig. 6. SEM of freeze-dried nanosilver ink.

The particle size distribution is similar to that of the initial nanosilver suspension. Therefore, the organic additives do not affect the stability of the nanosilver suspension. SEM images of freeze-dried nanosilver inks confirm the homogeneous dispersion of the nanoparticle in the ink (Fig. 6).

Consequently, the sedimentation rate through time does not exceed 1.1 wt.% over the course of 8 h (Fig. 7). Moreover, nanosilver ink appears to be more stable than a nanosilver suspension. This can be explained by the increase of the fluid media "solvent + additives mixture" viscosity [29].

The properties of the final ink are reported in Table III. The ink pH and conductivity are measured at 8.2 and 3.3 mS/cm, respectively, which is compatible with the selected printhead.

The ink exhibits a viscosity of 15.7 mPa·s through rheofluidifying flow behavior (Fig. 8). Indeed, at low shear

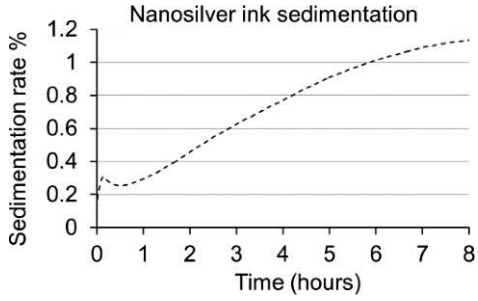

Fig. 7. Nanosilver ink sedimentation.

Table III
Nanosilver Ink Properties

Silver content (vol.%-wt.%)	5 35
pH	8.2
Conductivity at 25°C (mS/cm)	3.3
Viscosity at 20°C and 1000 s^{-1} (mPa·s)	15.7
Surface tension (mN/m)	41.5
Density	1.5
Ejection ratio	2.6
Sedimentation rate/8 h (wt.%)	1.1

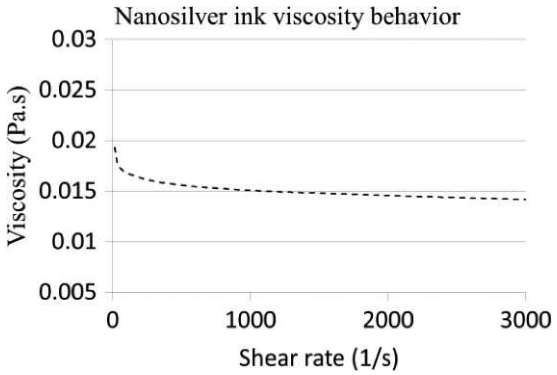

Fig. 8. Nanosilver ink rheological behavior.

rate, the ink viscosity indicates a shear thinning behavior, which disappears on increasing the shear rate. The viscosity is then constant from 100 to more than 1000 s^{-1}, and is compatible with printhead and jetting operating conditions.

The measured surface tension, 41.5 mN/m, is lower than the surface tension of the initial suspension, but too high compared with the printhead requirement. However, for the selected patterns for thick film application, a minimum track resolution of 50 μm is required, so that the surface tension is maintained at this value in order to reach a low spreading of the droplets on the alumina ceramic substrate. No significant variation was noted for ink characteristics after three months of aging. Therefore, the nanosilver ink is ready for printing and will be validated in terms of jetting behavior.

B. Nanosilver Ink Jetting Behavior

The printhead used for silver printing is an industrial printhead, which accommodates 256 nozzles with a 42 μm nozzle diameter and a 254 μm nozzle spacing. The printhead's aluminum reservoir was easily filled with the ink through a PALL 6 μm filter in order to remove potential dust and agglomerations, which could precipitate nozzle clogging. Ink was maintained in the reservoir by controlling the meniscus vacuum between 8 and 12 mbar. A purge of 1-2 s was applied to make the ink go through the nozzles, as an aid to priming. All 256 nozzles are electrically fired with a trapezoidal driven waveform of 75 V (Fig. 9), and a 5 μs pulse width with a slew rate of 70 V/μs. This pulse can be applied from 1 up to 8 kHz without any destabilization of the jetting behavior (i.e., no satellite droplets).

Using the DropAnalyser system, waveforms were adjusted in real time. When applying an adequate waveform, the printhead was scanned and the nozzles firing were detected as

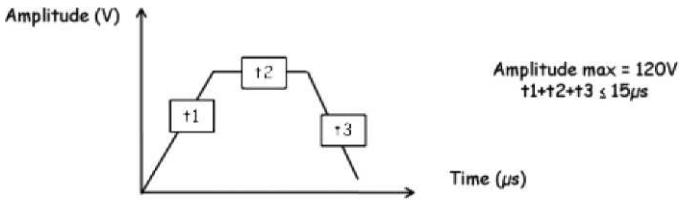

Fig. 9. Configuration of printhead electrical waveform.

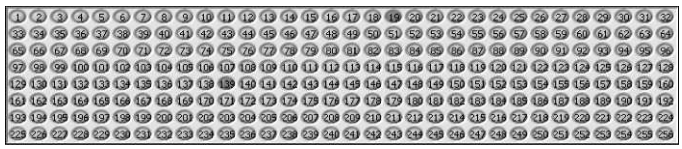

Fig. 10. Printhead nozzle firing detection with nanosilver ink.

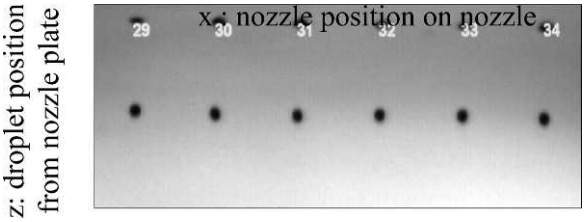

Fig. 11. Nanosilver ink jetting behavior.

shown in Fig. 10. The green dots are the fired nozzles recognized by the camera, whereas red dots are either not fired or not recognized. In fact, the recognition of the nozzles is helped by a prior printhead mapping with the detection of a circular shape by the camera through stroboscopic observation. One hour later, more than 98% of the nozzles are fired with a latency time higher than 10 min.

Moreover, the nozzle plate wetting was optimized, so that the surface tension, even though it is higher than the optimal specification (Table I) and combined with meniscus control, is convenient (Fig. 11). Silver nanoparticle jetting appeared to be stable and reproducible for all 256 nozzles.

With regard to printed electronic components, high resolution and regular and continuous lines are required. To reach this target, it is necessary to control some key parameters like ink formulation (viscosity and surface tension) and substrate nature (surface homogeneity, roughness, surface energy, and spreading). Another critical point is the control of the jetting parameters in order to minimize droplet positioning errors by reducing the droplet variation in volume, velocity, and vertical position (ΔZ), for both single nozzle and multiple nozzles. The

Table IV
Comparison of Droplet Vertical Position Variation (Z) for the printhead PZT Before and After Realignment

	Droplet ΔZ (μm) before realignment	Droplet ΔZ (μm) after realignment
All PZT	453	144.2
PZT_1	224.9	130.1
PZT_2	316.6	113.2
PZT_3	301.9	87.4
PZT_4	332.5	141.4

Table V
Nanosilver Droplet Main Characteristics

Mean Droplet Diameter (μm)	35
Mean Droplet Volume (pL)	23
Mean Droplet Velocity (m/s)	4
Mean Droplet ΔZ (μm)	80

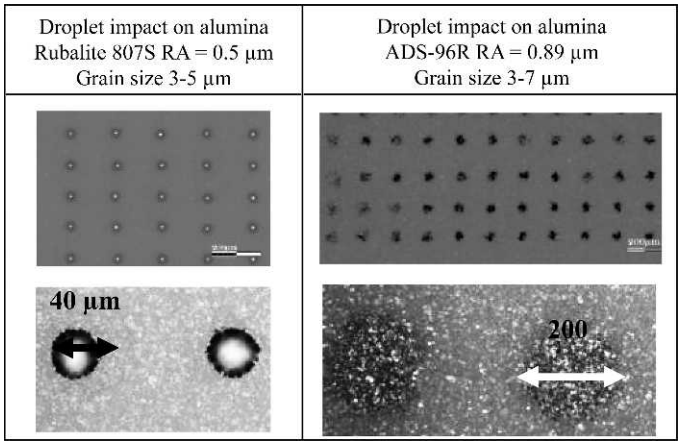

Fig. 12. Droplet impact as a function of substrate. Left substrate roughness of 0.5 μm, right substrate roughness of 0.89 μm.

CeraPrinter X-Serie offers the opportunity to reduce these positioning errors by adjusting the printhead electrical pulse in order to realign the four piezoelectric signals (PZT) for a group of 64 channels: for odd nozzles, PZT_1 (nozzle 1, 4, 9, up to 253) and PZT_3 (3, 7, 11, up to 255), and for even nozzles, PZT_2 (2, 6, 10, up to 252) and PZT_4 (4, 8, 12, up to 254) as shown in Table IV.

Another alternative to decrease ΔZ is to reduce the nozzle area by using all nozzles or a group of consecutive nozzles of the same PZT. Finally, the nanosilver ink exhibits a stable and reproducible ejection whose main jetting characteristics are summarized in Table V.

C. Droplet Impact on Alumina Substrate

For thick film application, the considered substrate is an alumina substrate. Printing occurs at a 500 μm distance between the printhead and the substrate to reduce the effect of the droplet jet straightness error.

The droplet impact strongly depends on the substrate roughness. Indeed, a 40 μm dot diameter was achieved on an alumina substrate with a roughness of 0.5 μm, with a regular circular shape and a 20 pL droplet volume. The impact of the same ink is irregular and inhomogeneous on the substrate with a roughness of 0.89 μm, with a variable dot diameter up to 200 μm (Fig. 12).

D. Design Filling

From the droplet impact diameter, different test vehicles were filled and simulated with the CeraSlice software by varying the different printing strategies according to the shape. The software gives the opportunity to customize the design (Fig. 13) with specific printing parameters (network, printing velocity, drying step, number of layers, etc.).

In the case of the designs simulated in Fig. 13, one layer of bond pads is achieved in four passes against 2 passes for lines. ; this was done to avoid the coffee staining effect and to control layer drying. Also, when the bond pad is perpendicular to the line, droplets can continue along the line right into the bond pad in order to guarantee continuity between the pad and the line. Indeed, we observed that drying shrinkage can make the intersection between the line and the pad very thin. On the Rubalite substrate, the dot spacing is adjusted to 36 μm in both the *X* and *Y* directions, so that the dot overlap was 4 μm. Each test vehicle is perfectly filled and ready to be printed.

E. Thick Film Component Printing and Optical Microscopy

The substrate was first air deionized and then fixed on the chuck before printing. A total of three layers were successively printed at 300 mm/s on the ceramic substrate at room temperature without any external drying.

Silver metallization exhibits a homogeneous and smooth surface without any cracks. According to each test vehicle design, a good definition is achieved (Fig. 14). The best line

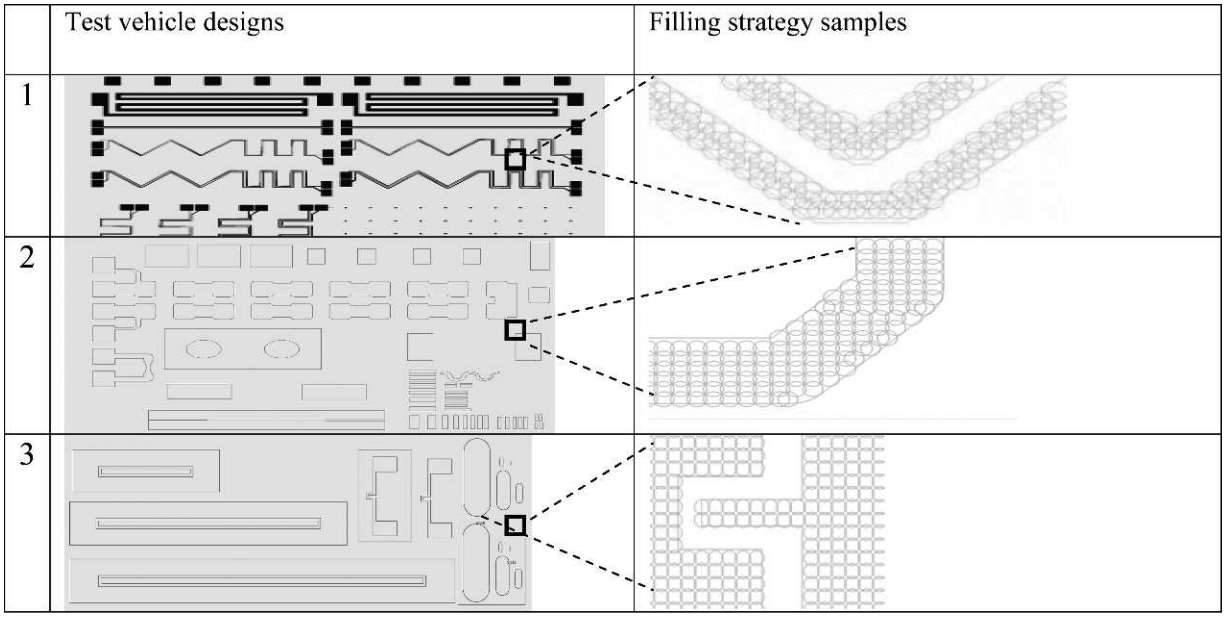

Fig. 13. Sample filling strategies for test vehicle designs.

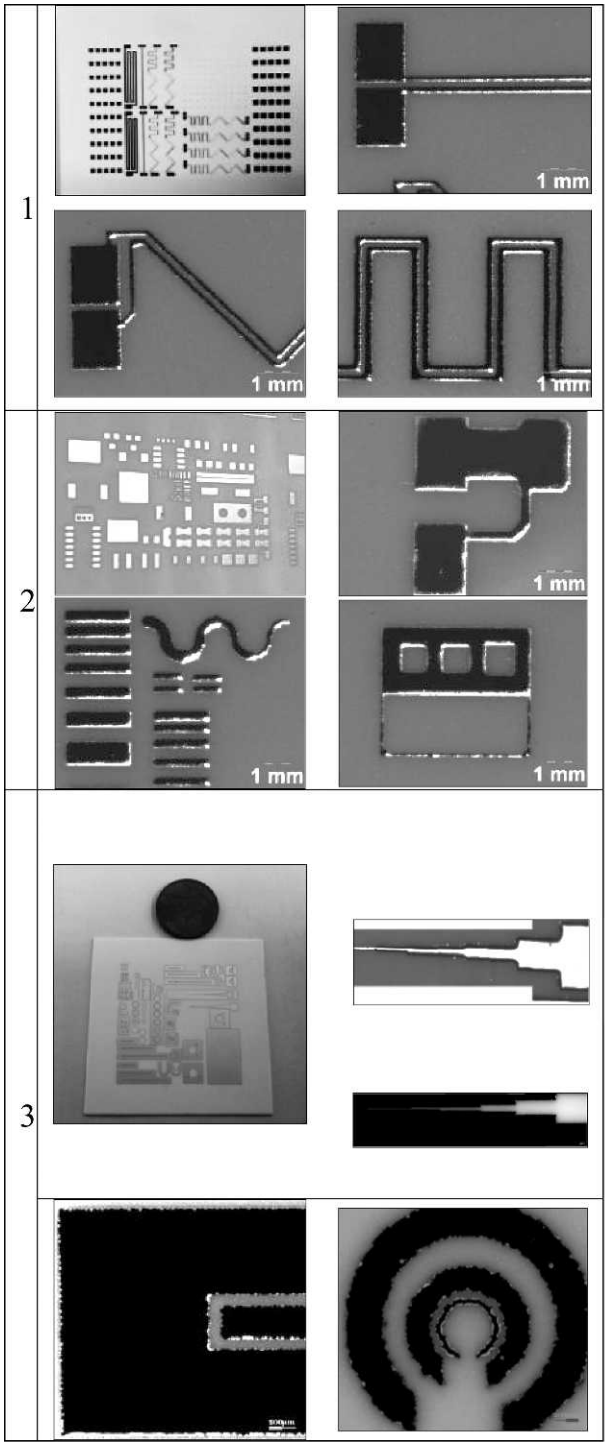

Fig. 14. Micrographs of printed test vehicles.

width and layer thickness for green deposit is estimated at 50 μm and 3 μm/layer, respectively.

F. Thermal Treatment and Electrical Performances

The silver contacts were sintered according to a standard hybrid thermal cycle at 850°C for 10 min in an IR industrial furnace. Indeed, these special nanoparticles get the correct conductivity at high temperature due to the presence of organic coating around them, which aids their aqueous dispersion. This coating is completely removed at high temperature, which can accept only substrate like glass or ceramic commonly used for thick film application. Moreover, to achieve high conductivity with metal densification, the thermal treatment should occur at a minimum temperature of 500°C. The fired thickness and shrinkage were estimated at 1.7 μm/layer and 20%, respectively. No cracks appeared during sintering. Furthermore, the presence of glass adhesion promoter allows the adhesion of the metal to the fired alumina substrate by glass bonding (melting point ~600°C). The contacts are 100% solderable with lead-free solder SAC405 95.5SN/4AG/0.5CU, and exhibit good adhesion on the substrate with a lift-off solderpad at 1.5 kg/mm^2 at 0H (0 hour without any aging test in oven (normally the aging occurs at temperature even for 48 h). Wire bonding was successfully realized with an ultrasonic wedge bonder 60 KHz-Delvotec 6400 using aluminum wire AlSi 1% 32 μm (Fig. 15). Previous investigations showed bad adhesion of the solderpad and alumina substrate when using ink without an adhesion promoter. Finally, the line conductivity was evaluated up to 10^7 S/m.

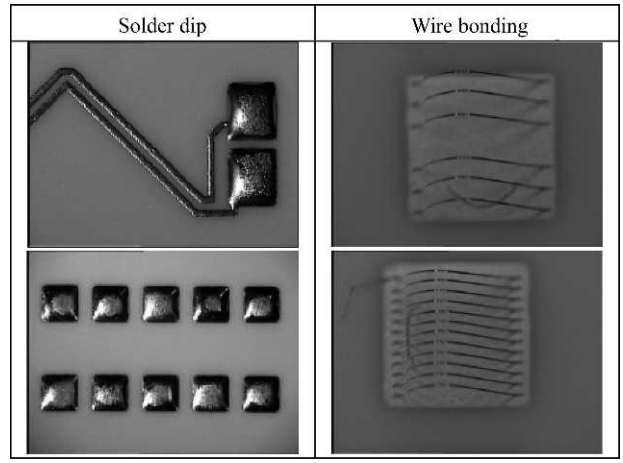

Fig. 15. Solderability and wire bonding tests.

G. Thick Film Demonstrators

According to the previous test vehicles printing feasibility and the exhibited good electrical properties for the silver material, small batches of thick film demonstrators were printed as shown in Fig. 16 on a large printing area (300 × 300 mm^2).

Silver metallization was also demonstrated on a 3D substrate with a good accuracy for a resonator (Fig. 17). The proposed structure (Fig. 17a) is a parallel plate dielectric resonator manufactured in a single part with two arms by 3D ceramic stereolithography process. This process was selected for its capacity to produce a 3D part made of low loss alumina ($\tan\delta \approx 10^{-4}$). The arms are used as a support for input and output microstrip lines. These lines create a magnetic field which can excite the fundamental TE101 mode rising at 27.71 GHz. This part is inserted into a brass cavity in order to provide an electromagnetic shield and a ground plane to the

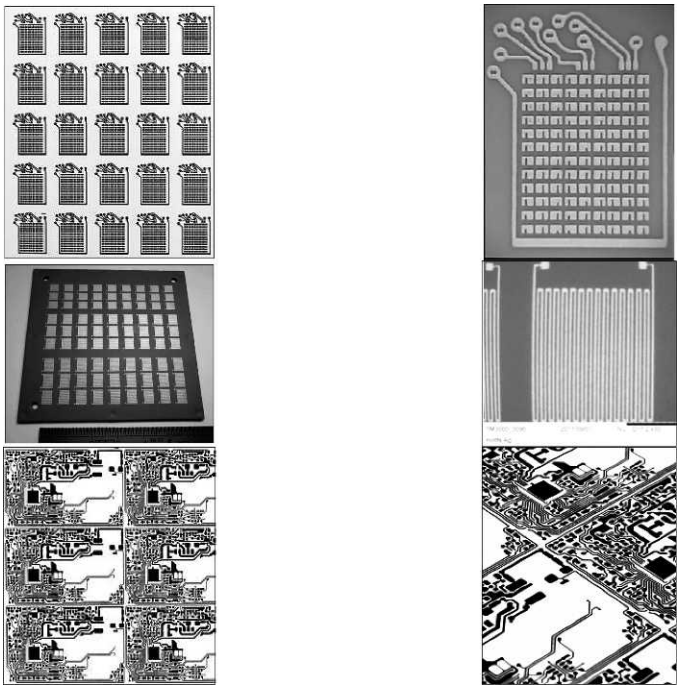

Fig. 16. Large area nanosilver 2D metallization demonstrations.

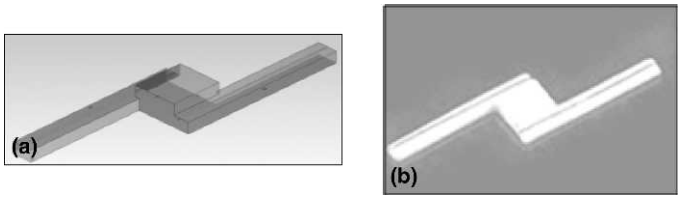

Fig. 17. Nanosilver 3D resonator (a) design and (b) printed line demonstration.

microstrip lines. Because the arms are at a lower level compared with the resonator top face, the patterning of the microstrip lines cannot be done with standard lithography techniques. Therefore, inkjet printing is a solution to create these lines. The typical conductivity observed with this structure for the microstrip lines is close to 2.5 S/μm. This value is close to the state of the art concerning the inkjet printing of silver particles and sufficient for the patterning of microwave guides. The typical accuracy observed is close to 20-30 μm, which is not as good as those obtained with a typical lithography process. However, as mentioned above, the 3D shape of the structure does not allow the proper use of this standard process. The observed accuracy is, however, acceptable for the patterning of microwave guides within this frequency range (27 GHz).

Finally, compared with traditional processing, IJP offers similar conductive properties and can be considered as a suitable process for thick film component manufacturing.

Inkjet Printing for MLCC Components

Inkjet printing is capable for substituting the traditional steps of tape casting, screen printing, and laminating in order to print electronic multilayer components with a single step of shaping by using several printheads dedicated to conductive

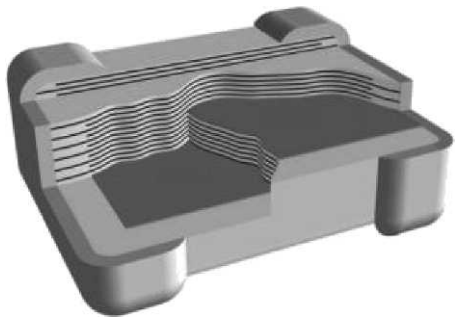

Fig. 18. Example of multilayer ceramic capacitor.

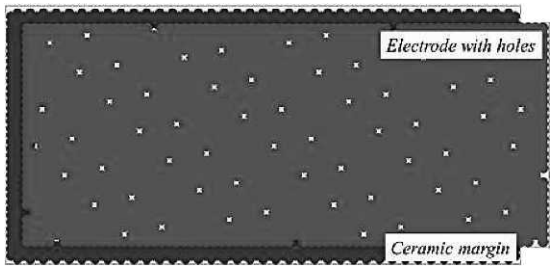

Fig. 19. Hole management within conductive layer.

and dielectric, or insulating, materials (Fig. 18). In industries of specific/custom electronic components with high added value, IJP can reduce the fabrication cost by 25% and offers new opportunities for new designs, high degree of integration, and better reliability. In addition, the inkjet printing process allows component miniaturization, in terms of component size. Moreover, this process gives high flexibility in terms of design, and therefore to achieve capacitors with complex architecture. Furthermore, thanks to inkjet printing accuracy, the dielectric margin width can also be reduced to about 100 μm (compared with around 500 μm for the standard serigraphy process), which contributes to the improvement in the MLCC properties.

MLCC designs can automatically be generated from CAD design information (shape and dimensions). Then, it is possible to adjust for each material (i.e., ceramic and metal in the case of MLCC components) the way to print the layers according to the material splat diameter (directly on the substrate or on the material of the previous layer), or its drying behavior (with the possibility to fill a complete layer in several passes or to add an IR flash drying pass between layers to aid in solvent evaporation).

It is also possible to generate some holes in the electrodes, to create ceramic bridges between the internal dielectric layers (Fig. 19), in order to prevent the electrodes from delaminating during the final MLCC cofiring. In addition, inkjet printing permits the printing of two different materials on the same layer, which means that the electrode thickness can be compensated by printing a ceramic layer around it, so that the global thickness is always the same on the whole surface of the component during manufacture.

A. Dielectric Material Preparation

I. Dielectric Suspension

The commercial powder selected is a magnesium titanate based dielectric (Type I) compatible with pure silver electrode

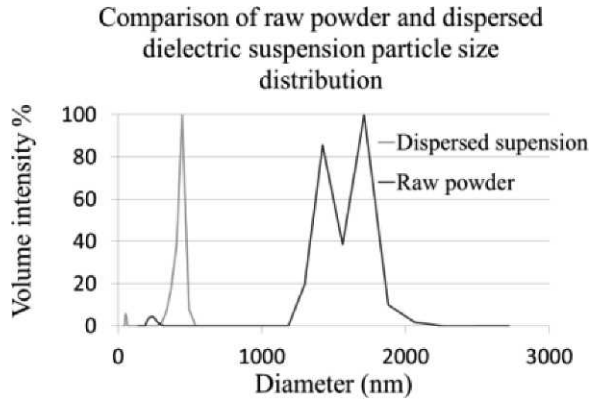

Fig. 20. Comparison of particle size distribution before and after milling.

Table VI
Dielectric Suspension Characteristics

Powder content (vol.%-wt.%)	25-75
Mean particles size (nm)	400
pH	10.5
Conductivity at 25°C (mS/cm)	6.2
Viscosity at 20°C and 1000 s^{-1} (mPa·s)	5.2
Surface tension (mN/m)	55
Density	1.7
Ejection ratio	9.9
Sedimentation rate/8 h (wt.%)	14.3

for cofiring at 950°C. The dispersion was performed in an aqueous media using a commercial anionic polyacrylic dispersant during 2 h attrition milling step. The milling helps to obtain a particle distribution with a D50 around 400 nm (Fig. 20).

Dispersant quantity was adjusted according to the IJP process specifications (Table I) to reach a minimum suspension viscosity and sedimentation rate. The dispersed suspension exhibited the physical characteristics mentioned in Table VI.

According to both printhead and inkjet printing requirements (Table I), the dielectric suspension is not adapted to the process, especially with regard to the surface tension and viscosity. Therefore, organic additives, namely, binder, plasticizer, and surfactant, were added to adjust the required properties.

II. Dielectric Ink Formulation

Different investigations were carried out to formulate high ceramic loading dielectric ink by adding binder, plasticizer, and surfactant to the previous stable suspension. The characteristics of the final ink formulation are shown in Table VII. One the one hand, binder and plasticizer help to increase the suspension viscosity from 5-17 mPa·s and give good mechanical strength to the printed green deposits. On the other hand, surfactant addition leads to a surface tension decrease, as expected. The sedimentation rate is better than the initial suspension and no big variation was detected on the different properties within 1 mo.

Table VII
Dielectric Ink Properties

Powder content (vol.%-wt.%)	15-40
Mean particle size (nm)	400
pH	10.3
Conductivity at 25°C (mS/cm)	3.73
Viscosity at 20°C and 1000 s^{-1} (mPa·s)	17.6
Surface tension (mN/m)	26.2
Density	1.5
Ejection ratio	1.9
Sedimentation rate/8 h (wt.%)	8.3

B. Dielectric Ink Jetting Behavior

The dielectric ink for MLCC application was ejected with an industrial printhead, which accommodates 256 nozzles orifices, with a 52 μm diameter and a spacing of 279 μm. The ink is introduced in a stainless tank (compatible with basic pH ink), going through a 6 μm PALL filter to remove potential dust and/or agglomerates; it is then maintained in the reservoir by controlling the meniscus vacuum at 10 mbar. To initiate ejection, several short purges (500 ms to 1 s) are applied. Thus, less than 90 min later, more than 93% of the nozzles are activated (Fig. 21).

Nevertheless, only a reduced portion of nozzles are necessary to print MLCC (about 30 nozzles for a 2 mm width component). When an adequate waveform is applied, the dielectric ink exhibits a stable and reproducible ejection for jetting frequencies from 0.5 up to 3 kHz. An example of jetting characteristics for this kind of ink is presented in Table VIII.

C. Design Simulation and Filling Strategy

For this study, the MLCC components are printed on a substrate which corresponds to a flexible, polymeric, 40 μm thick film. One benefit of using this substrate is that the final thermal treatment burns it away, so that the sintered MLCC can be retrieved separately.

First, both materials' (dielectric and silver) inks spreading behavior are characterized. Concerning the dielectric ink, the selected jetting pulse induces a regular splat diameter of 77 μm

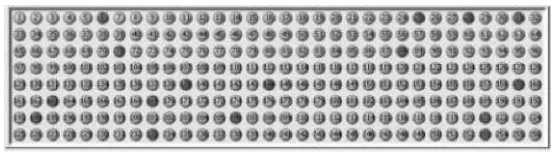

Fig. 21. Printhead nozzle firing detection with dielectric ink.

Table VIII
Dielectric Droplet Main Characteristics

Mean droplet diameter (μm)	45
Mean droplet volume (pL)	48
Mean droplet velocity (m/s)	2.7
Mean droplet ΔZ (μm)	115

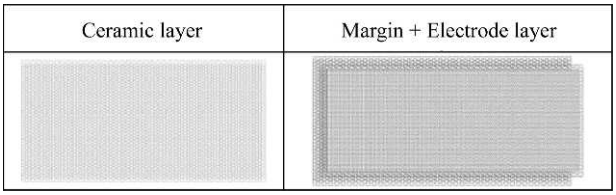

Fig. 22. Filling strategy for MLCC design.

on the substrate. The silver ink splat diameter is measured directly on a printed ceramic layer and not on the polymeric substrate, since the spreading behavior strongly depends on the substrate nature and metallic electrodes will be printed on dielectric layers. It is evaluated at 85 μm.

Secondly, starting from these parameters, the software allows the user to choose the way the shape will be filled by the droplets, in terms of splat network, number of ways to completely fill one layer, whether to work in return-mode or not, and so on. In addition, it is possible to adjust all of these parameters for each material (Fig. 22), since they generally do not behave the same way. In the case of the printed MLCC, the dielectric layers were printed in four passes and the silver layers in two passes, because of their drying behavior differences, but both in a hexagonal lattice to reach a good homogeneity in the layers. Furthermore, IR flash drying was applied regularly after each change of material.

D. MLCC Printing and Optical Microscopy

As mentioned above, the inkjet printing of MLCC components is a one step process, thanks to the use of two printheads for a unique fabrication, one containing the dielectric and one the silver ink. Thus, the bottom ceramic layer is first printed by successive layer stacking until the required thickness is reached, then the second printhead is automatically selected to directly print the metallic electrode on the ceramic; after that, an internal dielectric layer is printed, before another electrode, and so on, until the required number of internal electrodes is reached. Finally, a ceramic cover is printed to finish the component (Fig. 23).

As the printed dielectric layer thickness has been estimated to 5 μm/layer and 2 μm/layer for the silver one, a complete

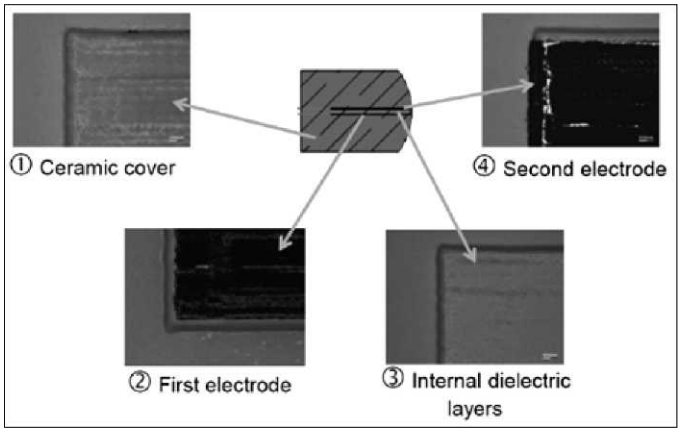

Fig. 23. MLCC printing steps.

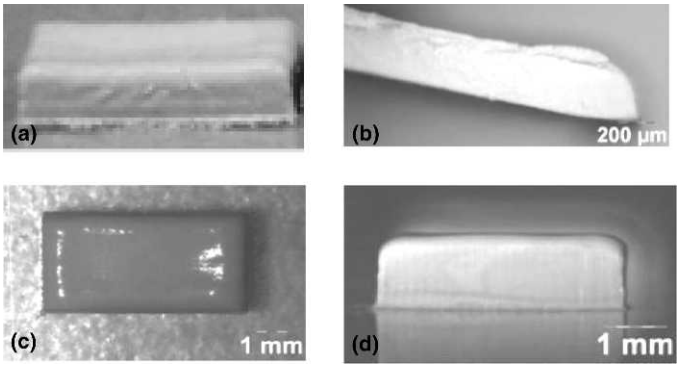

Fig. 24. (a-c) Green MLCC component. (d) Green dielectric cross section.

MLCC with 15 internal electrodes (and consequently 14 internal dielectric layers) corresponds to a 160 layer stack, and an approximately 800 μm high component with high green density for ceramic layers (Fig. 24). The component curvature can result from two phenomena: (1) the accumulation of solvent in the center of the component and (2) the difference in drying shrinkage between the top of the component and the interface layer with the substrate.

In addition, inkjet printing accuracy allowed for the production of MLCC with reduced margin width. That is how, combined with the ability of the CeraSlice software to realign one object with another, a ceramic margin of 120 μm in both *X* and *Y* directions was reached, as shown in Fig. 25.

Furthermore, the printing of a large amount of MLCC components in a unique fabrication was demonstrated: thus, 784 MLCC (regular spacing of 5 mm and 7 mm in *X* and *Y* directions, respectively) were printed on a 300 × 300 mm^2 wide printing area (Fig. 26) in less than 3 h. Therefore, we can assume that more than 1,000 components could be printed simultaneously by decreasing the space between the MLCC.

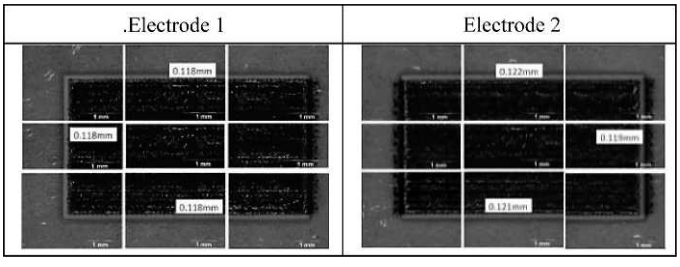

Fig. 25. Interdigital conductive layers on internal dielectric layer.

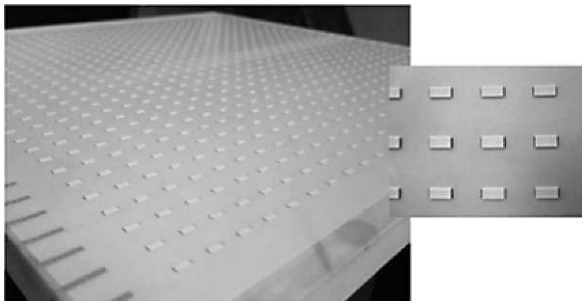

Fig. 26. MLCC large area printing.

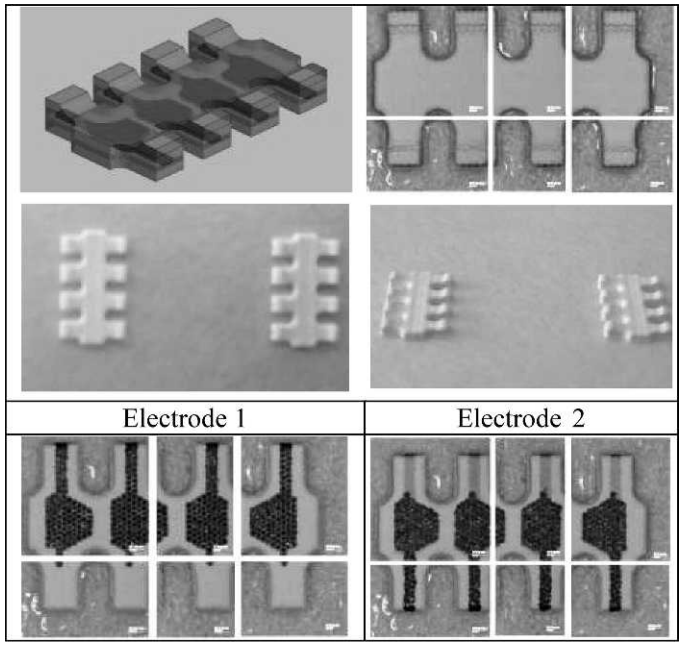

Fig. 27. MLCC complex shape.

Finally, as one of the main advantages of the inkjet printing process is its flexibility toward the required design, the feasibility of MLCC components with a more complex shape was proven (Fig. 27).

Indeed, as it is a numerical process, it is completely transparent for the user to print one type of MLCC or another; it is simply a matter of the CAD file being modified.

E. MLCC Sintering

The MLCC components made by an inkjet printing process are sintered at 960°C for 3 h, after burning out the organic additives at 400°C. Ceramic printed components sintered in the same conditions show very good density (Fig. 28), and a shrinkage in the *X*, *Y*, and *Z* directions of around 20%, 20%, and 30%, respectively. Moreover, the existing curvature previously mentioned in Section D above is more pronounced after sintering.

Nevertheless, the introduction of silver electrodes in printed MLCC generates delamination of the component after thermal treatment, due to the difference in shrinkage behavior for both materials, that is, ceramic and metal (Fig. 29).

To solve this mismatch, holes were incorporated in the silver electrodes (Fig. 30), which lead to ceramic bridges between the internal dielectric layers. In this fashion, MLCC components

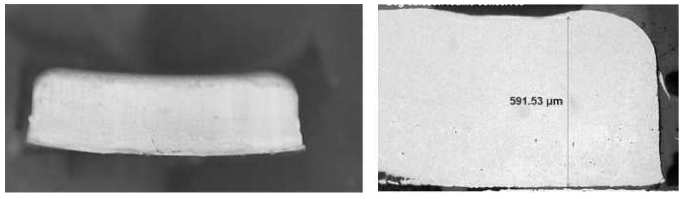

Fig. 28. Optical microstructure of dense sintered 3D dielectric component.

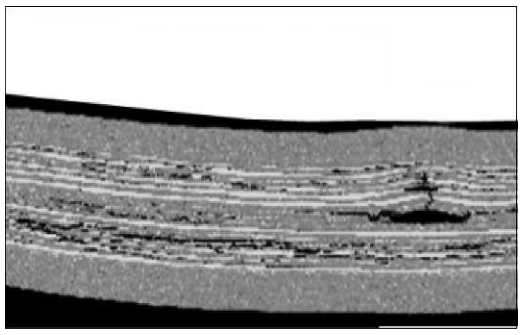

Fig. 29. Delaminated MLCC component with 15 layers of pure silver electrodes cofired at 960°C.

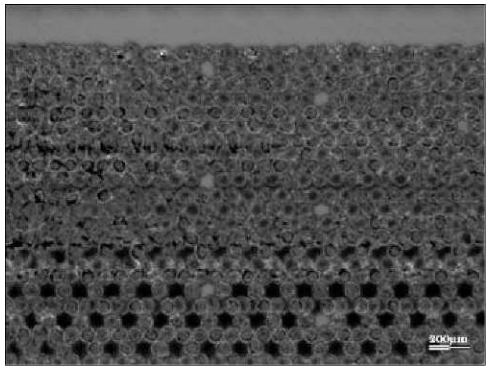

Fig. 30. Silver printed electrode with holes.

were successfully achieved with good cohesion without cracks after sintering at 960°C.

The MLCC components kept a regular shape with straight sides in the three dimensions (Fig. 31).

We note that the silver electrodes are still present in the MLCC after sintering, regularly spaced by the dielectric internal layers (Fig. 32) even if we observe a lack of metal in some areas of the cross section. The issue of delamination is no longer observed. Further dielectric measurements will allow conclusions to be drawn on the reliability of inkjet processing for the manufacture of MLCC components.

PERSPECTIVES

CeraDrop developments are focused on the one hand on the development of new materials in inks, especially nanogold and insulating inks for thick film applications. On the other hand, MLCC capacitor printing with new very low firing dielectric

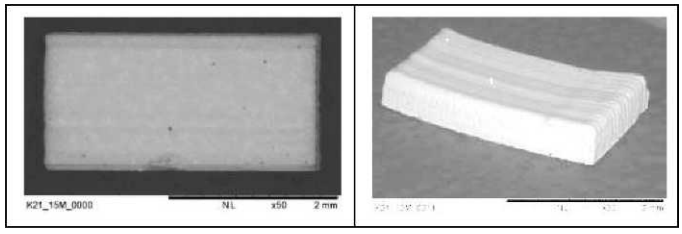

Fig. 31. Ceramic bridge sintered MLCC component.

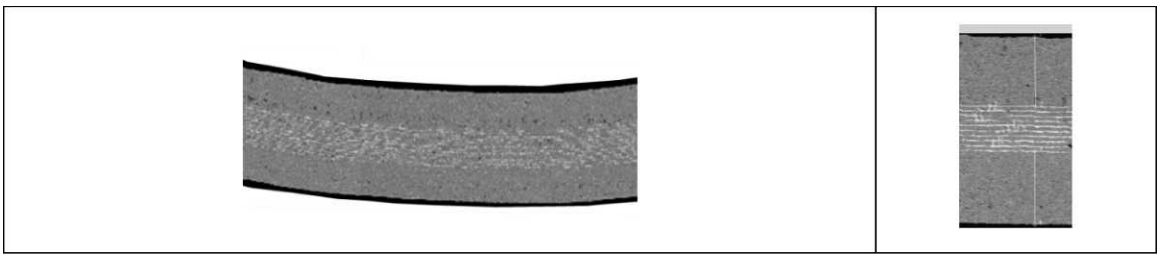

Fig. 32. Ceramic bridge sintered MLCC cross section.

powder (type II, for more capacitance), compatible with metallic alloys with low palladium content, are being investigated, for cofiring at very low temperature (around 930°C) to avoid electrode evaporation.

Conclusions

Highly concentrated conductive and ceramic aqueous inks have been formulated with a very stable behavior for inkjet printing technology using the CeraDrop 3D multimaterial printer. The nanosilver conductive ink was used for 2D ceramic metallization on 2D substrates and even on 3D substrates. Several parameters play a critical role for track definitions: the substrate, the ink jetting parameters, and the filling strategies (i.e., lattice, drying process). Adjustment of these different parameters allowed us to print high definition (50 μm) tracks on an alumina substrate. 3D Multilayer ceramic capacitors with 120 μm margins were successfully investigated with good control of the two printheads motion for dielectric and conductive inks, and droplet placement for each material. For both applications, the high flexibility of the technology helped us to print different designs, even for large area printing.

Acknowledgments

The authors thank the European Community, Region Limousin, and CNRS for their financial support and the industrial partners for their technical support and their participation in the present work.

References

[1] P.F. Blazdell, J.R.G. Evans, M.J. Edirisinghe, P. Shaw, and M.J. Binstead, "The computer aided manufacture of ceramics using multilayer jet printing," *Journal of Materials Science Letters*, Vol. 14, pp. 1562-1565, 1995.

[2] M. Mott, J.H. Song, and J.R.G. Evans, "Microengeneering of ceramics by direct ink-jet printing," *Journal of the American Ceramic Society*, Vol. 82, No. 7, pp. 1653-1658, 1999.

[3] M. Mott and J.R. Evans, "Zirconia/alumina functionally graded material made by ceramic ink-jet printing," *Materials Science and Engineering*, Vol. A271, pp. 344-352, 1999.

[4] Q.F. Xiang, J.R.G. Evans, M.J. Edirisinghe, and P.F. Blazdell, "Solid freeforming of ceramics using a drop-on-demand jet printer." *Proceedings of Institute of Mechanical Engineers/ Journal of Engineering Manufacture*, Vol. 211B, pp. 211-214, 1997.

[5] N. Reis, K.A.M. Seerden, B. Derby, J.W. Halloran, and J.R.G. Evans, "Direct ink-jet deposition of ceramic green bodies I-II," *Materials Research Society Symposium Proceedings*, Vol. 542, pp. 141-151, 1999.

[6] N. Reis, K.A.M. Seerden, B. Derby, J.W. Halloran, J.R.G. Evans, and P.S. Grant, "Ink-jet printing of wax-based alumina suspension," *Journal of the American Ceramic Society*, Vol. 84, pp. 2514-2520, 2001.

[7] N. Reis, B. Derby, and C. Ainsley, "Freeform fabrication by controlled droplet deposition of powder filled melts," *Journal of Materials Science*, Vol. 37, pp. 3155-3161, 2002.

[8] A.R. Bhatti, M. Mott, J.R.G. Evans, and M.J. Edirisinghe, "PZT pllars for 1-3 composites prepared by ink-jet printing," *Journal of Materials Science Letters*, Vol. 20, pp. 1245-1248, 2001.

[9] M.M. Mohebi and J.R.G. Evans, "A drop-on-demand ink-jet printer for combinatorial libraries and functionally graded ceramics," *Journal of Combinatorial Chemistry*, Vol. 4, No. 4, pp. 267-274, 2002.

[10] W.D. Teng and M.J. Edirisinghe, "Development of continuous direct ink jet printing of ceramics," *British Ceramic Transactions*, Vol. 97, No. 4, pp. 169-173, 1998.

[11] X. Zhao, J.R.G. Evans, M.J. Edirisinghe, and J.H. Song, "Ink-jet printing of ceramic pillar arrays," *Journal of Materials Science*, Vol. 37, pp. 1987-1992, 2002.

[12] A. Bertsch, "Microstéréolithographie par masquage dynamique," PhD Thesis, Institut National Polytechnique de Lorraine, France, 1996.

[13] C. Hinczewski, S. Corbel, and T. Chartier, "Ceramic suspensions suitable for stereolithography," *Journal of the European Ceramic Society*, Vol. 18, No. 6, pp. 583-590, 1998.

[14] F. Doreau, C. Chaput, and T. Chartier, "Stereolithography for manufacturing ceramic parts," *Advanced Engineering Materials*, Vol. 2, No. 8, pp. 493-496, 2000.

[15] C. Hinczewski, S. Corbel, and T. Chartier, "Stereolithography for the fabrication of ceramic three-dimensional parts," *Rapid Prototyping Journal*, Vol. 4, No. 3, pp. 104-111, 1998.

[16] T. Chartier, C. Chaput, F. Doreau, and M. Loiseau, "Stereolithography of structural complex ceramic parts," *Journal of Materials Science*, Vol. 37, No. 15, pp. 3141-3147, 2002.

[17] W.Q. Song, S.H. Masood, J.H. Hodgkin, and C. Freidl, "Development of metal-polymer composites for fused deposition modelling," *Proceedings of the 7th European Conference of Rapid Prototyping and Manufacturing*, pp. 79-85, 1998.

[18] G.M. Lous, I.A. Cornejo, T.F. McNulty, A. Safari, and S.C. Danforth, "Fabrication of piezoelectric ceramic/polymer composite transducers using fused deposition of ceramics," *Journal of the American Ceramic Society*, Vol. 83, No. 1, pp. 124-128, 2000.

[19] N.K. Tolochko, T. Laoui, L. Froyen, and V.I. Titov, "Fabrication of micromechanical components by laser sintering of fine powders," *Proceedings of the 10th European Conference on Rapid Prototyping and Manufacturing*, 2001.

[20] T. Muck, J. Fritz, and V. Wagner, "Better bottom contact properties in organic field-effect transistors with ultrathin layers," *Applied Physics Letters*, Vol. 86, p. 232101, 2005.

[21] T. Muck, V. Wagner, U. Bass, M. Leufgen, J. Geurts, and L.W. Molenkamp, "In situ electrical characterization of DH4T field-effect transistors," *Synthetic Metals*, Vol. 146, No. 3, pp. 317-320, 2004.

[22] E. Tekin, P.J. Smith, and U.S. Schubert, "Inkjet printing as a deposition and patterning tool for polymers and inorganic particles," *Soft Matter*, Vol. 4, No. 4, pp. 703-713, 2008.

[23] A. Kamyshny, M. Ben-Moshe, S. Aviezer, and S. Magdassi, "Ink-jet printing of metallic nanoparticles and microemulsions," *Macromolecular Rapid Communications*, Vol. 26, No. 4, pp. 281-288, 2005.

[24] B.-J. Gans, P.C. Duineveld, and U.S. Schubert, "Inkjet printing of polymers: State of the art and future developments," *Advanced Materials*, Vol. 16, No. 3, pp. 203-213, 2004.

[25] D. Kim and J. Moon, "Highly conductive ink jet printed films of nanosilver particles for printable electronics," *Electrochemical and Solid-State Letters*, Vol. 8, No. 11, pp. J30-J33, 2005.

[26] D. Kim, S. Jeong, B. Park, and J. Moon, "Direct writing of silver conductive patterns: Improvement of film morphology and conductance by controlling solvent compositions," *Applied Physics Letters*, Vol. 89, p. 264101, 2006.

[27] B. Park, D. Kim, S. Jeong, and J. Moon, "Direct writing of copper conductive patterns by ink-jet printing," *Thin Solid Films*, Vol. 515, No. 19, pp. 7706-7711, 2007.

[28] P. Calvert, "Inkjet printing for materials and devices," *Chemistry of Materials*, Vol. 13, No. 10, pp. 3299-3305, 2001.

[29] U. Currle and K. Krueger, "Observations on particle loaded silver inks," *Proceedings of the 16th European Microelectronics and Packagings Conference*, 2007.

[30] M. Lejeune, R. Noguera, C. Dossou-Yovo, and T. Chartier, "Ink-jet printing of ceramic micro-pillar arrays," *European Ceramic Society*, Vol. 29, No. 5, pp. 905-911, 2009.